Comparative Temperature Dependent Evaluation and Analysis of 1.2-kV SiC Power Diodes for Extreme Temperature Applications

Jinwei Qi, *Student Member, IEEE*, Xu Yang, *Senior Member, IEEE*, Xin Li, Wenjie Chen, *Senior Member, IEEE*, Kai Tian, *Student Member, IEEE*, Menghua Wang, Shuwen Guo, and Mingchao Yang

***Abstract*—Considering potential applications related to superconductivity and aerospace (typically less than 100 K), in this article, the temperature dependence of silicon carbide (SiC) power diodes is systematically characterized and analyzed over a wide temperature range of 90–478 K, especially focusing on cryogenic temperature. First, the static performance degradation mechanism of SiC diodes is established in an ultrawide temperature range, including forward/reverse I-V characteristics and junction capacitance (C_j) characteristics. Second, the reverse recovery characteristics are achieved, including peak reverse recovery current (I_{rm}), reverse recovery charge ($Q_{\rm rr}$), and switching energy ($E_{\rm sw}$), clarifying a clearer internal relationship between reverse recovery and junction temperature. Meanwhile, the aforementioned critical parameters are further analyzed on an electrical scale with normal atmosphere temperature, including switching speed range of 62.3–2054.8 A/μs, load current range of 6–30 A, and dc voltage range of 400–1000 V. Third, based on newly proposed power loss analysis method, the continuous operation performance of SiC diodes is quantified and analyzed in actual cryogenic converters. The excellent temperature dependence indicates that SiC diodes have great superiority for extreme applications. Importantly, SiC MOSFET's body diode shows the great potential to operate as a freewheeling diode in the compact converter, especially at cryogenic temperature.**

***Index Terms*—Buck converter, cryogenic temperature, reverse recovery performance, static performance, 1.2-kV silicon carbide (SiC) MOSFET's body diode (MBD), 1.2-kV SiC Schottky barrier diode (SBD).**

I. Introduction

With the widespread application of the electric system, more and more power conversion systems are required to work under extreme temperature conditions [1]–[6]. For example, the operating environment temperature of deep well exploration applications is higher than 400 K, while that is often less than 100 K for superconducting-related applications and aerospace applications. The extreme environment condition requires power devices to operate reliably over a large temperature scale. Meanwhile, due to the particularity of the aerospace applications (wide operating temperature, high system integration, and difficult replacement of elements), the reliability problem of power devices is extremely serious. Therefore, the electrical characteristics evaluation and analysis of power devices are very important.

Due to the superior material properties of silicon carbide (SiC) [7], SiC power devices have been an excellent candidate for high-power and high-frequency power conversion applications [8]–[11]. Currently, the SiC Schottky barrier diode (SBD) has been widely used instead of Si diode to increase the conversion efficiency and enhance the power density of the energy conversion system [10], [13], [24]. Moreover, the body diode of SiC MOSFET is potentially used as a freewheeling diode (FWD) for high power density and low system cost bidirectional energy conversion system [19].

With an extensive investigation in the utilization of SiC MOSFET's body diode (MBD), it can be found that the main limitations, using SiC MBD as a FWD in bidirectional power conversion system, come from two aspects: the forward degradation and reverse recovery loss. For the first issue, forward degradation is associated with the crystal defect called stacking fault. Fortunately, benefit from the development of industrial technology, the crystal material growth level of SiC material has been significantly improved in the last decade. At present,

Manuscript received October 14, 2019; revised January 6, 2020 and March 9, 2020; accepted April 20, 2020. Date of publication April 26, 2020; date of current version July 31, 2020. This work was supported in part by the National Key Basic Research Program of China (973 Program) under Grant 2015CB251004, in part by the Equipment Pre-Research Foundation under Grant 61409230511, in part by the National Natural Science Foundation of China under Grants 51625504, 61671368, and 51977175, and in part by the Shaanxi Natural Science Foundation under Grant 2014JM7277. Recommended for publication by Associate Editor J. Lam. *(Corresponding authors: Xu Yang; Xin Li.)*

Jinwei Qi is with the Department of Microelectronics School of Electronics and Information Engineering, Xi'an Jiaotong University, Xi'an 710049, China, with the State Key Laboratory of Electrical Insulation and Power Equipment, Xi'an Jiaotong University, Xi'an 710049, China, and also with the Department of Engineering–Electrical Engineering Division, University of Cambridge, Cambridge CB3 0FA, U.K. (e-mail: qijinwei@stu.xjtu.edu.cn).

Xu Yang and Wenjie Chen are with the State Key Laboratory of Electrical Insulation and Power Equipment, School of Electrical Engineering, Xi'an Jiaotong University, Xi'an 710049, China (e-mail: yangxu@mail.xjtu.edu.cn; cwj@mail.xjtu.edu.cn).

Xin Li is with the Department of Microelectronics School of Electronics and Information Engineering, Xi'an Jiaotong University, Xi'an 710049, China (e-mail: lx@mail.xjtu.edu.cn).

Kai Tian, Menghua Wang, Shuwen Guo, and Mingchao Yang are with the Department of Microelectronics, School of Electronics and Information Engineering, Xi'an Jiaotong University, Xi'an 710049, China (e-mail: tiankai@yahoo.com; wmh2394649077@stu.xjtu.edu.cn; guoshuwen@stu.xjtu.edu.cn; yangmingchao@mail.xjtu.edu.cn).

Color versions of one or more of the figures in this article are available online at https://ieeexplore.ieee.org.

Digital Object Identifier 10.1109/TPEL.2020.2990601

1.2-kV class SiC MOSFETs nearly show little sign of bipolar degradation caused by the body diode conduction, while the degradation issue still exists in higher voltage class SiC MOSFET (>3.3 kV) [33]–[37]. For the second issue, reverse recovery characteristics are related to the carrier modulation mechanism. It is strongly influenced by minority carrier lifetime, a temperature-dependent parameter. The poor reverse recovery performance not only produces large current overshoots during switching transients but also severely increases switching losses.

In order to explore the temperature robustness of SiC diodes, some research works have been carried out on temperature reliability analysis. They mainly focused on the high-temperature characteristics evaluation of SiC power diode [12]–[23].

As reported in some SiC diodes references associated with the temperature dependence of static characteristics, the forward current capability of the 600-V SiC SBD has little changed with temperature (even up to 450 °C), while series resistance of SiC SBD increases with temperature, resulting in a nonmonotonic change of forward voltage drop with increasing temperatures [12], [13]. For the body diode of SiC MOSFET, a different situation occurs while the diodes are characterized under a high temperature of 150 and 200 °C [14], [15], respectively. The leakage current of 1.2-kV SiC SBD, an important indicator representing reverse performance, increases with temperature from room temperature to 175 °C [16].

The reverse recovery characteristics of the power diode are extremely critical in the conversion system. The switching energy of SiC SBD has been shown as temperature invariant over a temperature range between −40 and 125 °C [17], [18]. For reverse recovery performance of body diodes, a worse case occurs, comparatively. The total reverse charge and peak reverse current of 1.2-kV SiC MBD increase with temperature, with a smaller temperature variation than that of 900-V Si CoolMOS over the temperature range of −75 to 200 °C [14], [19], [20]. Since the increase of reverse recovery charge limits the utilization of the body diode operating as a FWD [21], two technical solutions are introduced to eliminate this negative impact: adding antiparallel SiC Schottky diode in power leg [20] and developing advanced device technology [22], [23]. Currently, the reverse recovery behavior of latest generation 900-V SiC MOSFET has nearly been insensitive to temperature (up to 150°C) [22], only producing a small portion of switching losses, while the reverse recovery current peak of 1.2-kV double-trench SiC MOSFET is less sensitive to temperature compared with 1.2-kV planar SiC MOSFET [23].

However, unlike many high-temperature research works, few works have involved low-temperature properties of SiC power diodes, especially at cryogenic temperature. Considering the potential superconductivity-related application and aerospace application (often less than 100 K), the motivation of this article is trying to extend the research temperature of SiC power diodes to a wider temperature scale (from 90 to 478 K), especially focusing on the cryogenic temperature range.

The main contributions of this article are as follows.

1) The physical degradation mechanisms of static performance for SiC diodes are established based on semiconductor device physics in a very wide temperature range from 90 to 478 K (−183 to 205 °C), including forward/reverse *I–V* characteristics and reverse junction capacitance (C_j) characteristics. This will provide a good guideline for the future utilization of these kinds of components, especially under cryogenic temperature.
2) Three important recovery parameters are achieved and analyzed from 90 to 478 K with temperature control accuracy of 0.1 K, including peak reverse recovery current $(I_{\rm rm})$, reverse recovery charge $(Q_{\rm rr})$, and switching energy $(E_{\rm sw})$. The internal relationship between reverse recovery and junction temperature is much clearer. Furthermore, the high-frequency and high-power application potential of SiC power diodes are also validated over switching speed range of 62.3–2054.8 A/μs, load current range of 6–30 A, and dc voltage range of 400–1000 V.
3) The continuous operation reliability of SiC power diodes is verified based on two designed cryogenic hard switching nonisolated dc–dc buck over a temperature range from 90 to 298 K. A simplified method for accurate power loss analysis is proposed for cryogenic converters. The comparative characterizations experimentally demonstrate the application potential of SiC power diodes in cryogenic power conversion.

The devices under test in this article, including 1.2-kV SiC MOSFETs, 1.2-kV SiC SBD, and 900-V Si CoolMOS, are commercial high-voltage devices with similar current levels, as shown in Table I.

TABLE I
COMPARISON OF DEVICE PARAMETERS

Device technology	SiC MOS-A	SiC MOS-B	Si CoolMOS	SiC SBD
Breakdown Voltage (V)	1200	1200	900	1200
Continuous Forward Current (A) @ 25°C	17.7	22	15	15
Typical Diode Forward Voltage (V) @ 5A and 25°C	2.85	3.75	0.78	1.24
Continuous maximum drive voltage (V)	-10/+25	-6/+22	-20/+20	/

II. CLAMPED INDUCTIVE SWITCHING MEASUREMENTS

Double pulse test (DPT) circuit, as illustrated in Fig. 1, is widely used to characterize reverse recovery performance of power diode [25]. In this article, a 1.2 kV/36 A SiC MOSFET (C2M0080120D, manufactured by Wolfspeed) is selected as the auxiliary MOSFET while the bank capacitor (namely $C_{\rm bank}$) is set as 42.3 μF and a single layer air core load inductor ($L_{\rm load}$ of 334 μH) is designed with low parasitic. Particularly, to accurately characterize reverse recovery performance of power diode [26]–[29], parasitic parameter optimization is necessary and important, mainly including the minimization of power loop parasitic inductance (L_p) and driver loop parasitic inductance (L_g). After layout optimization, the power loop area and driver loop area in the DPT circuit are only 77.5 and 46.4 mm^2, respectively.

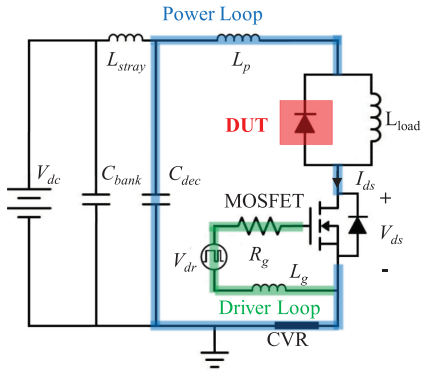

Fig. 1. Equivalent circuit schematic of DPT.

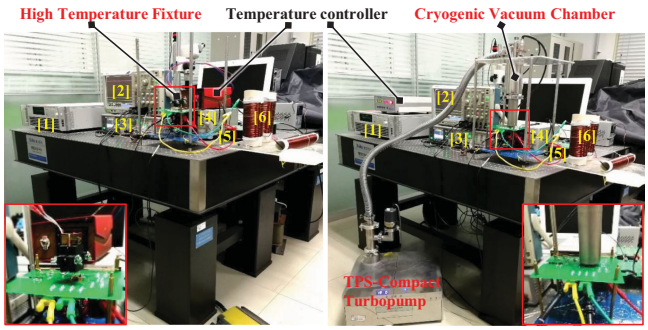

Fig. 2. (a) High and (b) cryogenic temperature characterization hardware with [1] programmable dc power supply, [2] digital phosphor oscilloscope, [3] pulse function arbitrary generator, [4] auxiliary power supply, [5] dc-link capacitor, and [6] load inductor.

As the dynamic characterization focuses on the temperature dependence of reverse recovery performance, a high-temperature fixture (a liquid nitrogen thermostat system) is designed and used to achieve precise temperature setup for high (low) temperature characterization, as shown in Fig. 2. The temperature control accuracy is only 0.1 K over the temperature range from 298 to 523 K (77 to 340 K). Noted that in the above temperature-dependent characterization system, only the DUTs are connected with a temperature control unit, heated by MCH alumina ceramic or cooled by liquid nitrogen. The rest circuit components and characterization equipment operate at room temperature, including the gate drivers, auxiliary MOSFET, $L_{\rm load}$, $C_{\rm bank}$, and decoupling capacitor $(C_{\rm dec})$. By eliminating the temperature influence on other components, the characterization system can normally operate and accurately measure target waveforms and parameters.

The double pulse switching waveforms are displayed and stored by Tektronix oscilloscope (DOP 4104B-L) with 0.4-ns sample interval and 1-GHz measurement bandwidth, and the switching current flowing through the auxiliary MOSFET is measured with a current view resistor (SSDN-414-01) with 400-MHz band-pass. The typical double pulse waveforms occurring on auxiliary MOSFET are illustrated in Fig. 3(a). Since the reverse recovery charge of SiC MOSFET-A's body diode (MBD-A), a current overshoot (up to 19.2 A) occurs at the

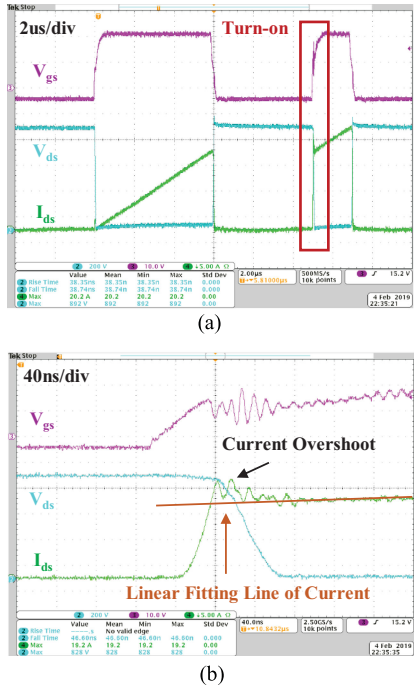

Fig. 3. (a) Double pulse waveforms and (b) zoom-in detail at turn-ON transient while taking the SiC MBD-A as freewheel diode: $R_g = 50\,\Omega$, $V_{\rm dc} = 800$ V, $I_{\rm load} = 15$ A, and $T_j = 298$ K. Scale: $V_{ds} = >200$ V/div, $V_{gs} = >10$ V/div, $I_{ds} = >5$A/div. Measured: current peak increases to 19.2 A at turn-ON transient.

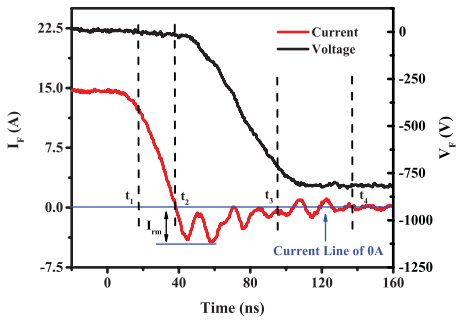

Fig. 4. Calculated switching waveforms of SiC MBD-A: $V_{\rm dc} = 800$ V, $I_{\rm load} = 15$ A and $T_j = 298$ K. Where t_1 and t_2 are the time that I_F falls to 90% and 0 of the forward current, respectively. And t_3 is the time that V_F falls to -90% of the bus voltage. t_4 is the time of 100 ns after t_2. Measured: peak reverse recovery current $(I_{\rm rm})$ is 4.173 A.

turn-ON transient, as shown in Fig. 3(b). The switching voltage and current waveforms occurring on power diode can be calculated, where the switching voltage is the difference between dc bus voltage and drain-source voltage $(V_{\rm ds})$ of auxiliary MOSFET, while the switching current is the difference between desired switching current level and the auxiliary MOSFET current. Particularly, the desired switching current should be obtained by linearly fitting ON-state current of auxiliary MOSFET, since the auxiliary MOSFET current slowly increases while auxiliary MOSFET is ON-state, as illustrated with the brown bold line in Fig. 3(b).

Based on the switching waveforms associated with reverse recovery performance, as shown in Fig. 4, many key parameters can be extracted, including peak reverse recovery current,

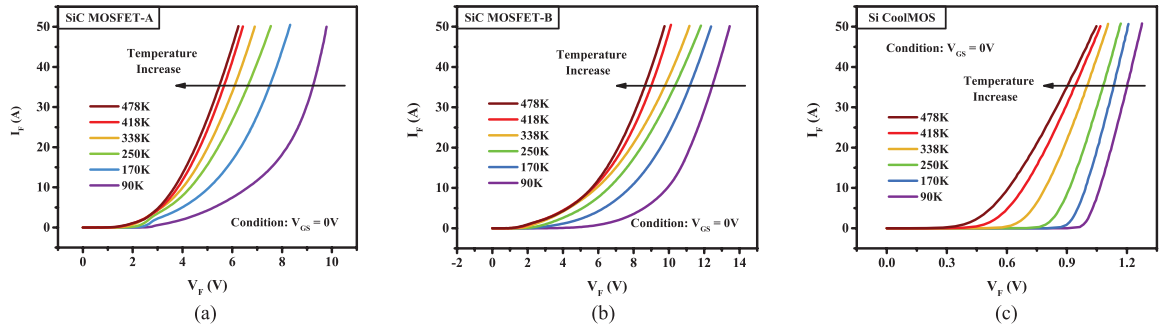

Fig. 5. Measured forward characteristics of (a) SiC MBD-A, (b) SiC MBD-B, and (c) Si CoolMOS's body diode with temperature increasing from 90 to 478 K. Measurement condition: $V_{\rm GS} = 0$ V.

reverse recovery charge, and switching energy loss. The reverse recovery charge can be calculated by integrating the forward current (I_F) of body diode, given by

$$Q_{\rm rr} = \int_{t_2}^{t_4} I_F dt. \tag{1}$$

To obtain accurate $Q_{\rm rr}$, the integration interval needs to be long enough to ensure that the forward current completely returns to 0, where the integration interval is 100 ns from t_2 (I_F falling to 0 A) to t_4. Meanwhile, the switching energy loss related to reverse recovery is calculated by integrating I_F and forward voltage (V_F) as

$$E_{\rm sw} = \int_{t_1}^{t_3} I_F * V_F dt \tag{2}$$

where the integration interval is t_1 (I_F falling to 90% of the forward current) to t_3 (V_F falling to -90% of the bus voltage).

Although the reverse recovery characterizations are conducted under different conditions (temperature, switching speed, current level, and voltage level), the analyzing and calculating methods are the same, as stated in the above part.

III. Static Performance Characterization

Based on the temperature controlling system composed of high-temperature fixture and liquid nitrogen thermostat unit, the static performance characterization platform is established by combining with the power device analyzer (Agilent B1505A). The static electrical properties of four power diodes, including forward characteristics, reverse characteristics, and junction capacitance characteristics, are characterized over the temperature range from 90 to 478 K. To quantify the measurement accuracy in this article, the experimental results are compared with the official electrical value extracted from the datasheet. Under the same test conditions and extraction methods, the absolute difference of forward voltage drop, reverse leakage current, and junction capacitance between the typical value in the datasheet and the measured value for SiC SBD are only 0.03 V, 13.7 uA, and 0.6 pF, respectively. The above good agreement indicates that the characterization system has sufficiently high accuracy for measuring static characteristics.

A. Temperature Dependence of Forward Characteristics

For three MBDs, including SiC SiC MBD-A, SiC MOSFET-B's body diode (SiC MBD-B), and Si CoolMOS's body diode (Si MBD), the forward characteristics are illustrated under different temperature in Fig. 5. It can be seen that the forward voltage drops of three-body diodes all decrease while the junction temperature increases from 90 to 478 K, indicating lower conduction energy loss at high temperatures.

The main physical mechanisms for the above performance drift come from two aspects. The first mechanism is related to the temperature dependence of the built-in voltage potential $(V_{\rm bi})$ of MBD [38], given by

$$V_{\rm bi} = \frac{kT}{q} \ln\left(\frac{N_A^- N_D^+}{n_i^2}\right) \tag{3}$$

where N_A^- and N_D^+ are the ionized impurity concentrations on the two sides of PN junction. The $V_{\rm bi}$ decreases with junction temperature due to the positive temperature coefficient of intrinsic carrier concentration (n_i). Evidently, the $V_{\rm bi}$ of SiC diodes (nearly 1.7 V at room temperature) is much larger than that for Si diode (nearly 0.7 V at room temperature) because of the far smaller intrinsic carrier concentration. The second mechanism is related to the temperature dependence of series resistance introduced by the drift layer, which has a negative temperature coefficient since the longer minority carrier lifetime will cause a deeper carrier modulation at higher junction temperature.

The forward characteristics of three MBDs under different gate bias voltages are illustrated in Fig. 6. For PiN diode (bipolar device), the injection level of hole carriers depends on the potential across the junction at the anode. The larger potential across the MOS channel with more negative gate bias leads to a larger voltage drop across the junction, resulting in more carrier injection [14]. Due to superior material properties (smaller intrinsic carrier concentration and larger critical electric field), SiC MOSFETs have much smaller drift region thickness and lager build in junction voltage compared with Si CoolMOS. Therefore, the negative gate bias voltages have a significant effect on the forward characteristics of SiC MBD, while that are virtually unaffected for Si MBD. The above results reveal that the gate voltage can be used to improve the forward characteristics of SiC MBDs, which is important and critical to reduce forward conduction losses in a bidirectional power conversion system.

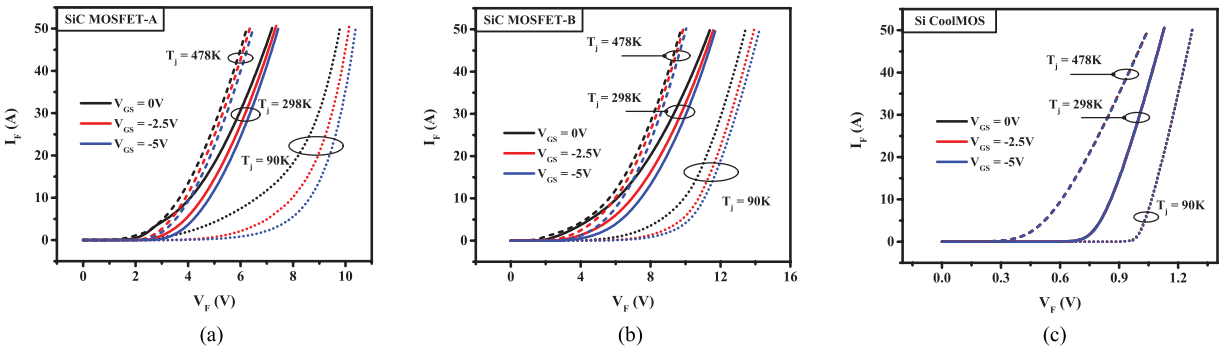

Fig. 6. Measured forward characteristics of (a) SiC MBD-A, (b) SiC MBD-B, and (c) Si CoolMOS's body diode with gate bias voltage of 0, −2.5, −5V. Measurement conditions of temperature: T_j = 90 , 298, and 478 K.

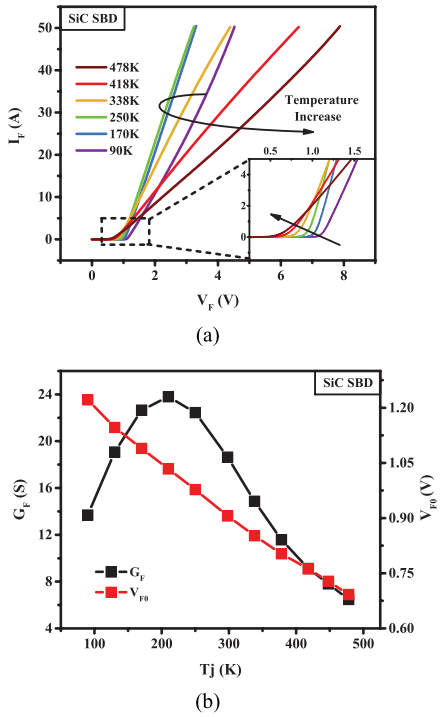

Fig. 7. (a) Measured forward characteristics of SiC SBD. (b) Extracted temperature dependence of forward conductance (G_F) and forward intercept voltage (V_{F0}) over temperature range from 90 to 478 K.

The temperature influence on SiC SBD is different from body diodes as illustrated in Fig. 7. In high mobility semiconductors, the thermionic emission theory can be used to describe the current flow across Schottky barrier interface. When a forward bias is applied on SBD, the forward current is calculated by [38]

$$I_F = I_{s0} * e^{\frac{qV_{\rm FS}}{nkT}} \tag{4}$$

where $V_{\rm FS}$ is the forward voltage drop across the schottky contact, n is the ideality factor, k is the Boltzmann's constant, T is the absolute temperature, and I_{s0} is the saturation current, given by

$$I_{s0} = AT^2 e^{-\frac{q\Phi_{\rm BN}}{kT}} \tag{5}$$

where A is the effective Richardson's constant, and $\Phi_{\rm BN}$ is the Schottky barrier height.

Under small $V_{\rm FS}$ condition, the I_F is mainly determined by the Schottky barrier height. As the temperature increases, the lower Schottky barrier height corresponds to the smaller built-in voltage of SiC SBD, which ultimately results in a good linear relationship between the forward intersect voltage (V_{F0}) and the temperature, as shown in the drawing of partial enlargement of Fig. 7. The V_{F0} decreases from 1.22 to 0.69 V with a negative temperature coefficient of −1.366 mV/K over the temperature range from 90 to 478 K.

Under the larger $V_{\rm FS}$ condition, SBD enters high-current conduction mode, the I_F is mainly determined by the $V_{\rm FS}$. The forward conductance (G_F) of SiC SBD can be obtained by calculating the slope of forward *I–V* curves, where the G_F increases from 13.68 S to 23.80 S under the temperature range from 90 to 210 K, then decreases down to 6.47 S at 478 K. Due to the existence of the incomplete ionization effect for SiC device, the effective carrier concentration in the drift region dramatically decreases under lower temperature, particularly at a cryogenic temperature [39]. In comparison, the carrier mobility has a maximum value between 100 to 200 K [40], indicating that the positive and negative temperature coefficient occurs on both sides of the temperature point corresponding to the maximum carrier mobility. As a result, the drift region conductance $(\sigma_{\rm drift})$ shows a nonmonotonic temperature-dependent relationship with a maximum value, resulting in a minimum value of total series-specific resistance of SiC power SBD. Eventually, the G_F exists a maximum peak on the temperature scale, approximately 200 K, as illustrated in Fig. 7(b).

Considering the temperature dependence of both V_{F0} and G_F comprehensively, the forward voltage drop of SiC SBD will show a nonmonotonic change with a minimum value on the temperature scale, indicating that the forward characteristics of SiC SBD are degraded at cryogenic temperature. For all evaluated power diodes, the temperature dependence of forward voltage with the current level of 15 A (V_{F_15A}) is extracted and illustrated in Fig. 8. When the temperature increases from 90 to 478 K, the V_{F_15A} of Si MBD decreases linearly from 1.123 to 0.675 V with a temperature coefficient of −1.155 mV/K. At the same time, the V_{F_15A} of SiC MBD-A (SiC MBD-B) monotonically decreases from 7.574 to 4.146 V (from 10.648

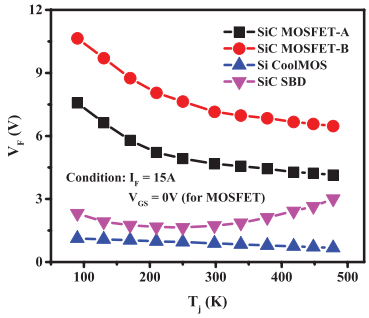

Fig. 8. Extracted temperature dependence of the forward conduction voltage over temperature range from 90 to 478 K. Measurement conditions: $V_{\rm GS} = 0$ V (for three MOSFETs), $I_F = 15$ A.

to 6.470 V). On the contrary, the V_{F_15A} of SiC SBD shows a nonmonotonic temperature dependence related to V_{F0} and G_F, where the V_{F_15A} decreases from 2.317 to 1.642 V under the temperature range from 90 to 250 K, then increases up to 3.005 V at 478 K.

While the SiC MBD is used as a FWD in practical bidirectional power conversion circuits, the time duration that all switching current flows through the body diode is only dead time, which is a small part of the entire switching period [30], [31]. Consequently, the conduction energy loss produced on SiC MBD does not show a significant increase whereas the V_{F_15A} of two SiC MBDs is larger than that of Si MBD and SiC SBD, especially at cryogenic temperature.

B. Temperature Dependence of Reverse Characteristics

During the avalanche breakdown of power devices, it is a common practice to find the voltage at which the ionization integral becomes equal to unity [7]. The negative temperature coefficient of impact ionization coefficients causes a lager depletion region width at higher temperatures [32]. Consequently, the breakdown voltage of power devices will increase with temperature.

The temperature dependence of reverse characteristics on four DUTs is shown in Fig. 9. The breakdown voltage of SiC MBD-A (SiC MBD-B) linearly increases from 1655.01 to 1729.98 V (2249.94 to 2394.97 V) over the temperature range from 90 to 478 K, while the breakdown voltage of Si MBD also linearly increases from 765.28 to 1165.02 V over a slightly smaller temperature range from 90 to 448 K. Due to the differences in material properties, the increase rate of breakdown voltage for two SiC MBDs (0.193 and 0.374 V/K, respectively) is much smaller than that of Si MBD (1.117 V/K). Furthermore, as the leakage current increases rapidly with an intrinsic carrier concentration of semiconductor, the SiC power devices show smaller leakage current compared with Si power devices due to the lower intrinsic carrier concentration. At 448 K, the leakage current of SiC MBDs is less than 1 μA while that of Si MBD is larger than 50 μA, indicating that the SiC diodes are more suitable for wide temperature applications.

In comparison, the reverse characteristics of SiC SBD are also characterized and analyzed over the temperature range from 90 to 478 K. The leakage current of SBD is comprised of three

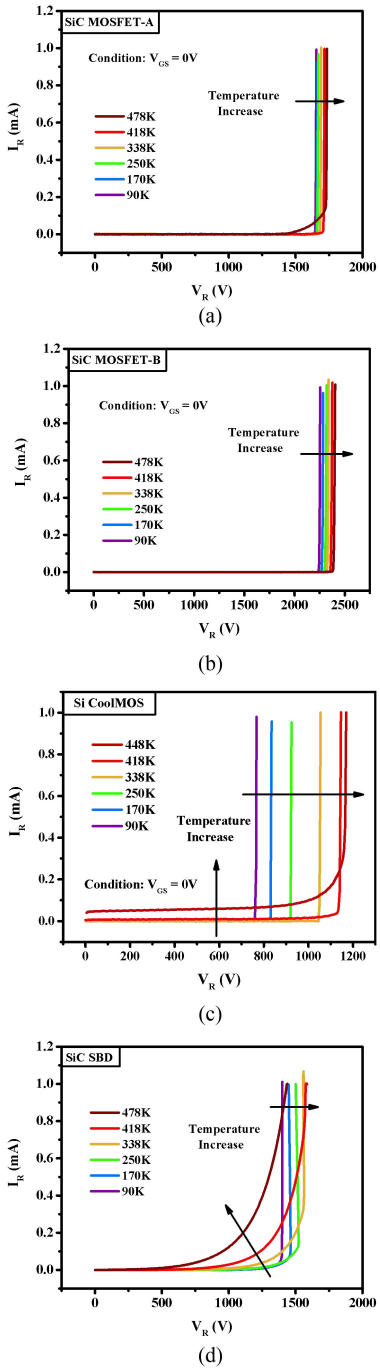

Fig. 9. Measured reverse characteristics of (a) SiC MBD-A, (b) SiC MBD-B, (c) Si CoolMOS's body diode, and (d) SiC SBD with temperature increasing from 90 to 478 K. Measurement condition: $V_{\rm GS} = 0$ V (for three MOSFETs).

components: space-charge generation current, diffusion current, and thermionic emission current, however, the thermionic emission component is dominant due to the relatively small barrier height [7]. Consequently, the reverse current (I_R) of SBD related about thermionic emission mechanism is a strong function of the Schottky barrier height and the temperature, given by

$$I_R = -I_{s0} * \left(e^{-\frac{qV_R}{kT}} - 1\right) \tag{6}$$

where I_{s0} is the saturation current and calculated by the formula (5), V_R is reverse bias voltages. Therefore, the I_R of SBD not only exponentially increases with reverse bias voltage but also exponentially increases with junction temperature. The characterization results show that the I_R of the SiC SBD increases from 5.23 μA (at 90 K) to 308.12 μA (478 K) with the reverse bias voltage of 1200 V.

Above characterization and analysis indicate that the reverse characteristics of SiC MBDs are better than that of Si MBD and SiC SBD over a wider temperature range, since the less leakage current results in the smaller reverse power dissipation, especially at high temperatures.

C. Temperature Dependence of Junction Capacitance

As illustrated in Fig. 10, the temperature dependence of DUTs' junction capacitance (C_j) is characterized over temperature range from 90 to 478 K. While power diode is in reverse biased state, the reverse-blocking voltage is supported across depletion region, and the depletion region width (W_D) is related to the applied reverse bias voltage (V_R) [38], given by

$$W_D = \sqrt{\frac{2\varepsilon_s}{qN_D}(V_R + V_{\rm bi})} \tag{7}$$

where $V_{\rm bi}$ is the built-in voltage, ε_S is the dielectric constant of semiconductor, and N_D is the doping concentration of the drift layer. The junction capacitance associated with the depletion region is given by

$$C_j = A_j \frac{\varepsilon_s}{W_D} \tag{8}$$

where A_j is the effective junction area of power diode [38].

Due to the presence of the JFET region in power MOSFET, the effective depletion layer width will suddenly change under a certain reverse voltage range, eventually resulting in a sudden change of C_j. The above phenomenon can be observed in Fig. 10, where the reverse voltage corresponding to the C_j sudden change is 12.89, 1.53, and 43.95 V, respectively, for SiC MBD-A, SiC MBD-B, and Si MBD. In contrast, the above phenomenon of C_j sudden change does not exist for SiC SBD.

As described by formula (7) and (8), the space charge region continues to expand while the reverse voltage increases from 0.15 to1000 V. As a result, the C_j of SiC MBD-A (SiC MBD-B) decreases from 794.95 (1672.18) to 46.57 pF (47.23 pF), while the C_j of SiC SBD reduces from 808.53 to 35.51 pF at room temperature. Similarly, the C_j of Si MBD reduces from 19025.5 to 35.41 pF with V_R range from 0.15 to 800 V. Noted that a larger chip area of Si MBD results in a much higher C_j while comparing with three SiC devices. And the difference between the C_j of two types of devices is more pronounced under the low reverse bias voltage conditions.

The formula in (7) illustrates that the depletion region width is related to built-in voltage of junction and reverse bias voltage. The negative temperature coefficient of the built-in junction voltage will produce a larger C_j at a lower temperature. While the reverse bias voltage is small, the W_D is dominated by $V_{\rm bi}$ under low reverse voltage. Therefore, the temperature influence

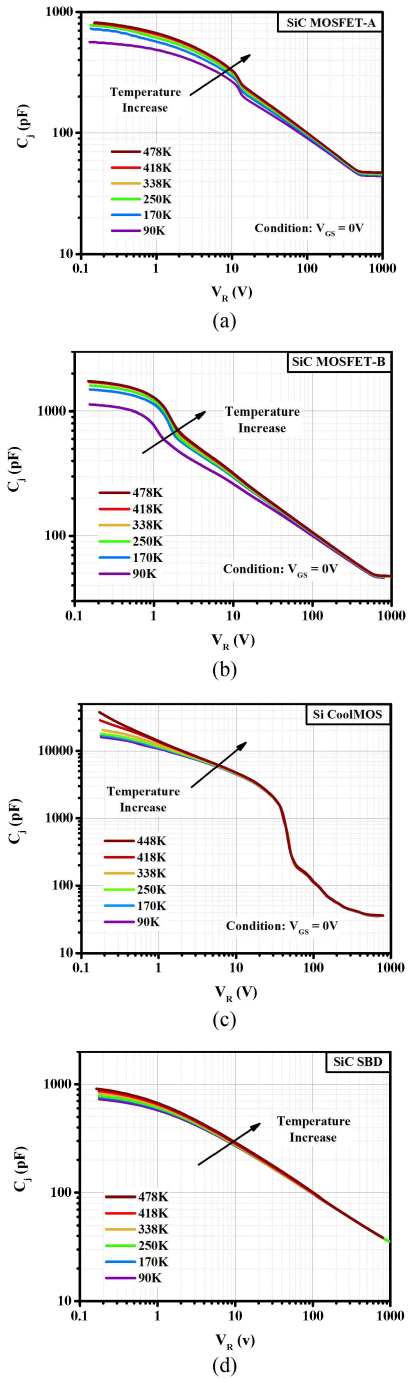

Fig. 10. Measured junction capacitance of (a) SiC MBD-A, (b) SiC MBD-B, (c) Si CoolMOS's body diode, and (d) SiC SBD with temperature increasing from 90 to 478 K. Measurement condition: $V_{\rm GS} = 0$ V (for three MOSFETs).

on C_j for all DUTs is more pronounced under low reverse voltage conditions.

The junction capacitance, as a parasitic parameter, is critical to the switching process in the energy conversion circuit, which not only affects the switching speed but also causes additional energy loss. The characterization results indicate that the SiC diodes own smaller junction capacitance and are more suitable for high-speed and high-frequency applications. Furthermore, the temperature decrease helps to reduce junction capacitance and increase switching speed.

IV. Reverse Recovery Performance Characterization

The reverse recovery performance of power diode is a critical characteristic for the power conversion application, which not only affects the current overshoot at switching transient but also has a serious impact on the switching energy loss of conversion system. In this section, the temperature dependence characterization of reverse recovery performance is conducted and analyzed over the temperature range from 90 to 478 K. Moreover, to make a benchmark and clearly illustrate the relative dependence strength of temperature while comparing with the dependence strength of other electrical conditions, the reverse recovery performance is fully investigated under whole electric conditions, including the switching speed dimension, current level dimension, voltage level dimension, and temperature dimension. Under the same test conditions and extraction methods as mentioned in the datasheet, the small absolute difference of reverse recovery charge, 5.59 nC, indicates that the characterization system has a sufficiently high accuracy of reverse recovery measurement. In order to make a comparative characterization, all the measurements of four diodes are done with the same DPT board combined with the temperature controlling system.

A. Temperature Dependence of Reverse Recovery Performance

Considering the actual application conditions of 1.2-kV power devices, the three 1.2 kV SiC diodes are characterized by the following conditions: dc bus voltage ($V_{\rm bus}$) of 800 V, load current ($I_{\rm load}$) of 15 A, and temperatures range from 90 to 478 K. In comparison, the characterization conditions of 900 V Si CoolMOS's body diode are $V_{\rm bus}$ of 600 V, $I_{\rm load}$ of 15 A, and temperatures range from 90 to 448 K, respectively. While conducting temperature dependence characterization, sufficient time has been given before conducting each measurement to ensure the DUTs' temperature attaining equilibrium with the temperature controlling fixture's temperature, varied by using liquid nitrogen thermostat system (and high-temperature fixture), increasing from 90 K to room temperature (and room temperature to 478 K).

During the turn-OFF process of power diode, the stored charge, producing from the carrier modulation mechanism, needs to be removed to support bus voltage. A higher switching speed (*di/dt*) means the stored charge is removed faster, causing an increase in the stored charge distribution gradient in the drift region, ultimately resulting in a larger reverse recovery current peak. Noted that if the $I_{\rm rm}$ is too larger, the diode will be damaged because of the too high internal temperature of the power device. For reverse recovery characterization of Si MBD, a small *di/dt* of 62.3 A/μs is chose to prevent Si MBD from being damaged by large $I_{\rm rm}$, corresponding gate resistance of 620 Ω. Unfortunately, the $I_{\rm rm}$ of Si MBD has exceeded 46 A even a small switching speed was chosen, which is nearly 1.35 times the maximum forward pulse current (34 A) listed in the DATASHEET. For the characterization of SiC diodes, the *di/dt* increases up to 527.8 A/μs by using gate resistance of 50 Ω.

The temperature dependence of reverse recovery waveforms on four DUTs is illustrated in Fig. 11. For two SiC MBDs, the waveform shifts caused by temperature are reflected in two

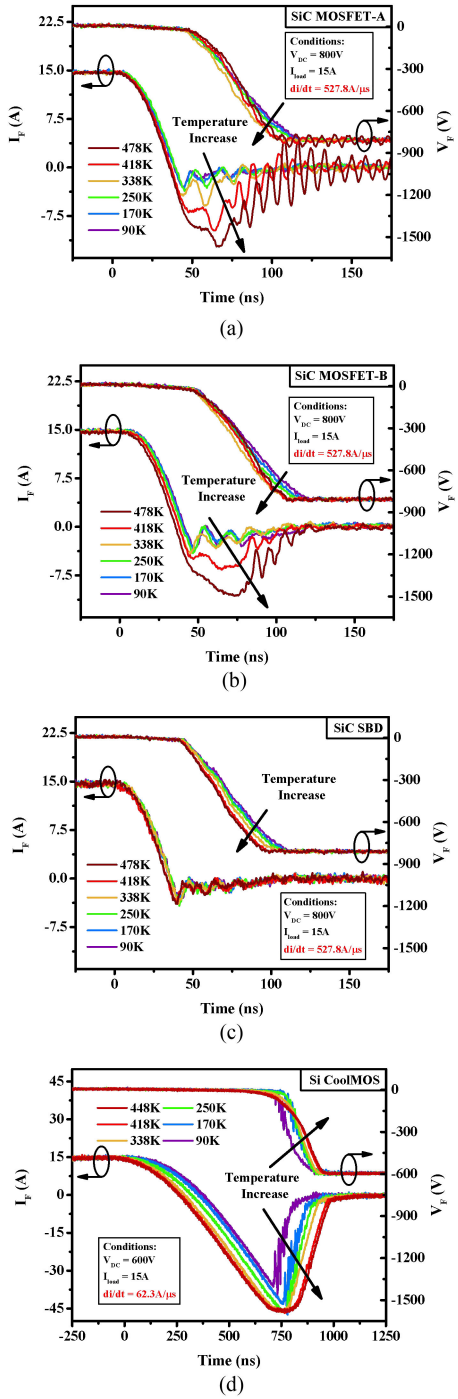

Fig. 11. Measured reverse recovery waveforms of (a) SiC MBD-A, (b) SiC MBD-B, and (c) SiC SBD with temperature increasing from 90 to 478 K, similarly the waveforms of (d) Si CoolMOS's body diode with temperature increasing from 90 to 448 K. Measurement condition: $V_{\rm GS} = 0$ V (for three MOSFETs operating as freewheeling diode).

aspects. First, the reverse recovery current of two SiC MBDs has significantly deteriorated with junction temperature increase, especially in the high-temperature range. Second, the positive temperature coefficient of voltage dropping ratio causes a shorter time of voltage dropping phase, where the voltage dropping ratio (*dv/dt*) of SiC MBD-A (and SiC MBD-B) increases from 11.68 to 14.95 V/ns (and from 11.85 to 14.55 V/ns) over the

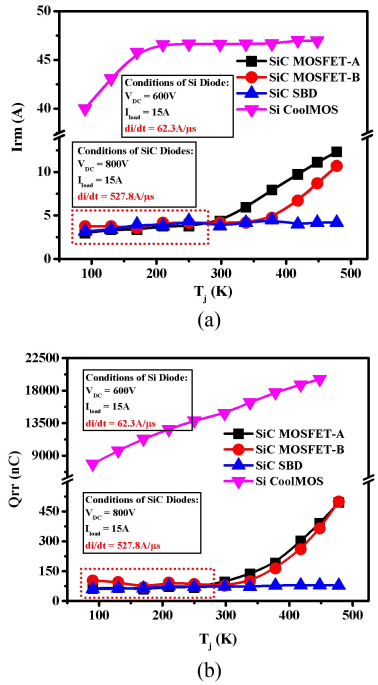

Fig. 12. Extracted temperature dependence of (a) peak reverse recovery current ($I_{\rm rm}$) and (b) reverse recovery charge ($Q_{\rm rr}$) of four DUTs over temperature range from 90 to 478 K. Measurement condition: $V_{\rm GS} = 0$ V (for three MOSFETs operating as freewheeling diode).

temperatures range from 90 to 478 K. For Si MBD, a similar situation occurs over the temperature range from 90 to 448 K, but the reverse recovery current deteriorates much more than that of two SiC MBDs, especially the $I_{\rm rm}$ larger than 46.97 A at 448 K. In contrast, the reverse recovery current of SiC SBD is almost no change under different temperature, where only the voltage drop ratio slightly increase from 12.8 to 16.0 V/ns over the temperature range from 90 to 478 K.

Based on the above-mentioned measurement results associated with reverse recovery, the temperature dependence of three key parameters (peak reverse recovery current, reverse recovery charge, and switching energy) are extracted with the extraction method described in Section II.

For bipolar devices, the reverse recovery characteristics are severely related to the minority carrier lifetime, the shorter minority carrier lifetime at a lower temperature will help improve reverse recovery performance of power diode. By comparison, the reverse recovery characteristics of unipolar devices are almost immune to temperature because there is no carrier modulation mechanism related to the minority carrier lifetime.

As illustrated in Fig. 12, the $I_{\rm rm}$ and $Q_{\rm rr}$ of four diodes have positive temperature coefficient over the temperature range from 90 to 478 K. Particularly, under low-temperature range (<298 K), the $I_{\rm rm}$ and $Q_{\rm rr}$ of two SiC MBDs are almost unaffected by temperature and comparable to that of SiC SBD (shown by the red square), indicating the great potential for cryogenic power conversion application. The $I_{\rm rm}$ of SiC MBD-A (and SiC MBD-B) is nearly about 4.16 A with variation of 0.36 A (and 3.82 A with variation of 0.50 A) while that of SiC SBD is 3.79 A with variation of 1.2 A. Similarly, the $Q_{\rm rr}$ of SiC MBD-A

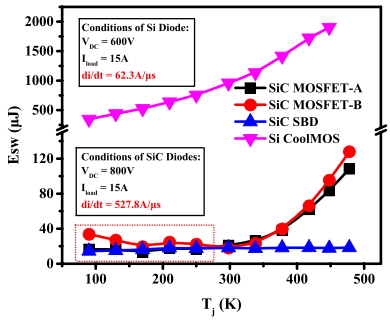

Fig. 13. Extracted temperature dependence of switching energy loss ($E_{\rm sw}$) of four DUTs over temperature range from 90 to 478 K. Measurement condition: $V_{\rm GS} = 0$ V (for three MOSFETs operating as freewheeling diode).

(and SiC MBD-B) is nearly about 67.17 nC (and 85.93 nC) while that of SiC SBD is 66.68 nC. In contrast, the $I_{\rm rm}$ and $Q_{\rm rr}$ of two SiC MBDs significantly increase when the junction temperature is higher than room temperature, meaning that the high-temperature environment is not conducive to the SiC MBDs utilization. The $I_{\rm rm}$ of SiC MBD-A (and SiC MBD-B) rapidly increases from 4.34 to 12.32 A (and from 4.17 to 10.70 A) while that of SiC SBD only increases by 0.41 A from 3.78 to 4.19 A. Meanwhile, the $Q_{\rm rr}$ of SiC MBD-A (and SiC MBD-B) increases from 95.97 to 495.65 nC (and from 76.65 to 500.49 nC) while that of SiC SBD only increases by 5.04 nC from 72.78 to 77.82 nC. For reverse recovery characterization of Si MBD, the absolute value and temperature coefficient of $I_{\rm rm}$ and $Q_{\rm rr}$ are much larger than that of SiC diodes even though the switching speed of Si MBD is only 62.3 A/μs smaller than that of SiC diodes (527.8 A/μs). The $I_{\rm rm}$ and $Q_{\rm rr}$ of Si MBD increase up to 46.97 A and 19.60 μC at 448 K.

As illustrated in Fig. 13, the temperature dependence of switching energy loss is nearly consistent with the $I_{\rm rm}$ and $Q_{\rm rr}$. Noted that the $E_{\rm sw}$ of two SiC MBDs is comparable to that of SiC SBD under the temperature range from 90 K to room temperature, as shown by the red square. Due to the shorter minority carrier lifetime at a lower temperature, the $E_{\rm sw}$ of SiC MBD-A (and SiC MBD-B) is only 16.48 μJ (and 33.72 μJ) at the temperature of 90 K, while the $E_{\rm sw}$ of SiC SBD (as a unipolar device) is hardly affected by temperature and is only 16.46 μJ with the variation of 4.05 μJ. In comparison, the $E_{\rm sw}$ of Si MBD is 54 times higher of SiC diodes at 298 K around.

The above characterization results show that SiC diodes offer advantages compared with Si MBD over a wide temperature range. Especially, the small $E_{\rm sw}$ of two SiC MBDs indicates that SiC MBDs have a potential to operate as FWDs in cryogenic applications, whose circuit is advantageous for achieving high conversion efficiency while increasing power density of the energy conversion system.

B. Switching Speed Dependence of Reverse Recovery Performance

The switching speed dependence characterization is carried out, in this part, the *di/dt* regulation in the range from 62.3 to 2054.8 A/μs is implemented by adjusting the R_g of auxiliary

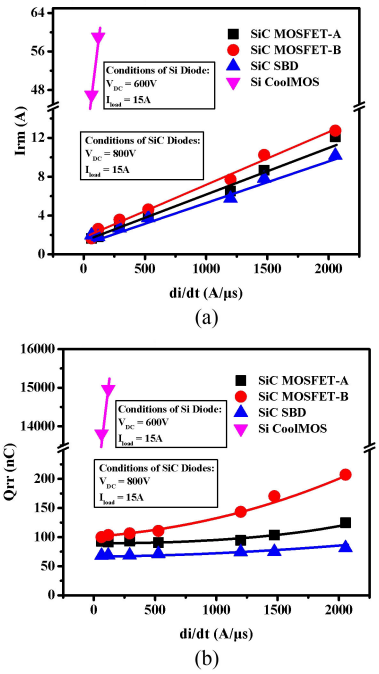

Fig. 14. Extracted switching speed dependence of (a) peak reverse recovery current ($I_{\rm rm}$) and (b) reverse recovery charge ($Q_{\rm rr}$) of four DUTs over *di/dt* range from 62.3 to 2054.8 A/μs. Measurement conditions: $T_j = 298$ K, $V_{\rm GS} = 0$ V (for three MOSFETs operating as freewheeling diode).

MOSFET from 620 to 5 Ω. The measurement conditions are set as follows: the $I_{\rm load}$ of 20 A, and the $V_{\rm bus}$ of 800 V (and 600 V) for SiC diode (and Si diode).

The faster removing speed at higher *di/dt* causes an increase of minority carrier concentration gradient in the drift region, resulting in the shorter reverse recovery time and larger peak reverse recovery current. The characterization conditions for all DUTs should be the same for comparative experiments, but the measurements of Si MBD are only conducted under two switching speed condition since the Si MBD is completely damaged when the switching speed is greater than 292.7 A/μs, where the $I_{\rm rm}$ is more than 100 A.

As illustrated in Fig. 14, the switching speed dependence of $I_{\rm rm}$ and $Q_{\rm rr}$ is measured and extracted over the switching speed range from 62.3 to 2054.8 A/μs. The measured results show that the $I_{\rm rm}$ of four DUTs linearly increases with switching speed. The $I_{\rm rm}$ of SiC MBD-A (and SiC MBD-B) increases from 1.64 to 12.13 A (and 1.65 to 12.75 A) while that of SiC SBD increases from 1.97 to 10.19 A. In comparison, The $I_{\rm rm}$ of Si MBDs are 47.00 and 59.02 A much larger than that of three SiC diodes with *di/dt* conditions of 62.3 and 118.1 A/μs. Moreover, the $Q_{\rm rr}$ increases with *di/dt* in accordance with the $I_{\rm rm}$ characteristics. For three SiC diodes (SiC MBD-A, SiC MBD-B, and SiC SBD), the increment of $Q_{\rm rr}$ are 32.06, 107.07, and 13.16 nC. In comparison, a worse situation occurs on Si MBD where the absolute value of $Q_{\rm rr}$ exceeds 13.8 μC even at a very low switching speed condition of 62.3 A/μs.

The switching speed dependence of $E_{\rm sw}$ is calculated and shown in Fig. 15. The *di/dt* change has a small effect on the $E_{\rm sw}$ of three SiC diodes compared with Si MBD. The $E_{\rm sw}$ variation of SiC SBD (SiC MBD-A and SiC MBD-B) is only 9.20 μJ (18.58 and 18.64 μJ) over whole *di/dt* range, while the $E_{\rm sw}$ of Si MBD is larger than 668 μJ with *di/dt* of 62.3 A/μs. The small $E_{\rm sw}$ of SiC SBD and two SiC MBDs demonstrates the application potential over switching speed scale, especially, accompanying an optimum operating speed for SiC MBDs. The above results quantitatively verify that SiC diodes are more suitable for high-frequency applications.

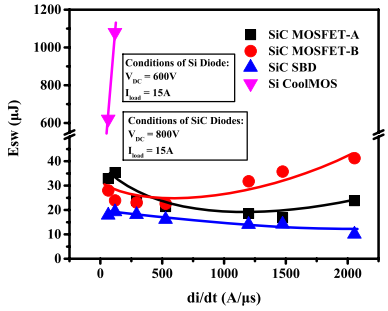

Fig. 15. Extracted switching speed dependence of switching energy loss ($E_{\rm sw}$) of four DUTs over *di/dt* range from 62.3 to 2054.8 A/μs. Measurement conditions: $T_j = 298$ K, $V_{\rm GS} = 0$ V (for three MOSFETs operating as freewheeling diode).

C. Current Level Dependence of Reverse Recovery Performance

The current level dependence characterization is conducted to estimate the reverse recovery performance under different current levels. The measurement conditions used in this part are like the previous experiment. The bus voltage is set to 800 V for SiC diodes while that of Si MBD is 600 V. Meanwhile, the switching speed is adjusted to 527.8 A/μs and 62.3 A/μs for SiC diodes and Si MBD.

The current level dependence of $I_{\rm rm}$ and $Q_{\rm rr}$ is extracted with the load current increasing from 6 to 30 A. As shown in Fig. 16, the $I_{\rm rm}$ and $Q_{\rm rr}$ of two SiC MBDs are hardly affected by the current level, nearly about 4.62 A and 90.52 nC for SiC MBD-A (4.60 A and 99.32 nC for SiC MBD-B), correspondingly, 3.64 A and 64.39 nC for SiC SBD. In comparison, the $I_{\rm rm}$ of Si MBD almost linearly increases by 19.29 A from 37.57 to 56.86 A and the $Q_{\rm rr}$ increases by13.222 μC from 8.658 to 21.88 μC.

As shown in Fig. 17, the switching losses are extracted over the current range from 6 to 30 A. The impact of current changes on two aspects must be considered. First, the energy stored in the parasitic inductance will be released during the current drop phase, and the more energy is released as the current level increases. Second, the larger forward current slightly enhances the switching speed, eventually resulting in an increase in energy loss. When the three SiC diodes operate with a switching speed of 527.8 A/μs, the parasitic inductance related energy release is larger than the increase of energy loss because of a faster switching speed under high current condition. Therefore, the $E_{\rm sw}$ of SiC MBD-A (SiC MBD-B) slightly reduces from 19.38 to 17.59 μJ (from 22.03 to 17.80 μJ) with the variation of 1.79 μJ (4.23 μJ). Meanwhile, the $E_{\rm sw}$ of SiC SBD reduces from 17.40 to 9.11 μJ. By contrast, the switching speed related loss increase of Si MBD dominates under the high current condition. Under

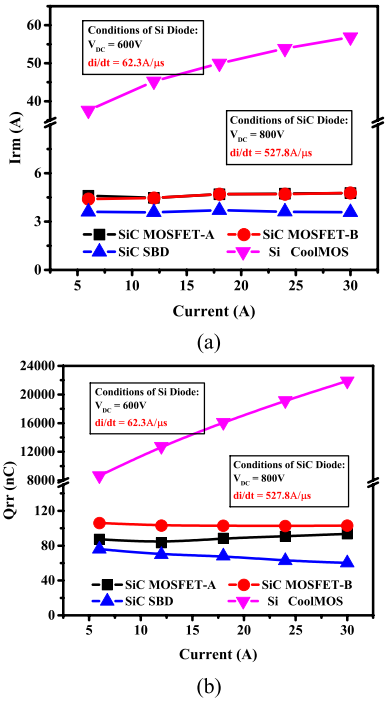

Fig. 16. Extracted current level dependence of (a) peak reverse recovery current ($I_{\rm rm}$) and (b) reverse recovery charge ($Q_{\rm rr}$) of four DUTs over current range from 6 to 30 A. Measurement conditions: $T_j = 298$ K, $V_{\rm GS} = 0$ V (for three MOSFETs operating as freewheeling diode).

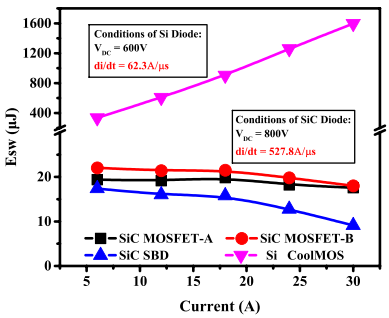

Fig. 17. Extracted current level dependence of switching energy loss ($E_{\rm sw}$) of four DUTs over current range from 6 to 30 A. Measurement conditions: $T_j = 298$ K, $V_{\rm GS} = 0$ V (for three MOSFETs operating as freewheeling diode).

the switching speed condition of 62.3 A/μs, the $E_{\rm sw}$ increases up to 1.597 mJ and the variation is larger than 1263 mJ.

Considering the negative current coefficient of $E_{\rm sw}$ and the almost constant $I_{\rm rm}$, a larger switching current contributes to the enhancement of energy conversion efficiency, resulting in a higher power density.

D. Voltage Level Dependence of Reverse Recovery Performance

The reverse recovery characterizations are conducted under different voltage levels to estimate voltage dependence of reverse recovery performance. The bus voltage for 1.2 kV SiC diode increases from 600 to 1000 V while that for 900 V Si MBD increases from 400 to 800 V. The switching current is chosen as 15 A and the switching speed is adjusted to 527.8 A/μs for SiC diodes (and 62.3 A/μs for Si MBD).

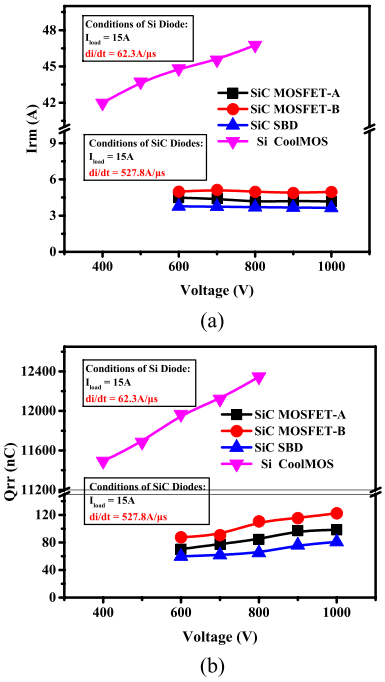

Fig. 18. Extracted voltage dependence of (a) peak reverse recovery current ($I_{\rm rm}$) and (b) reverse recovery charge ($Q_{\rm rr}$) of four DUTs over reverse voltage range from 400 to 1000 V. Measurement conditions: $T_j = 298$ K, $V_{\rm GS} = 0$ V (for three MOSFETs).

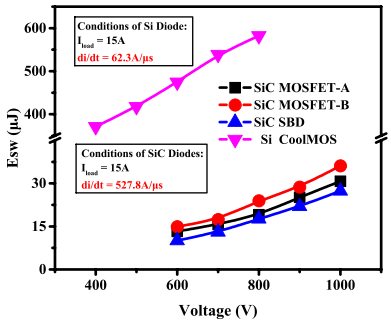

Fig. 19. Extracted voltage level dependence of switching energy loss ($E_{\rm sw}$) of four DUTs over reverse voltage range from 400 to 1000 V. Measurement conditions: $T_j = 298$ K, $V_{\rm GS} = 0$ V (for three MOSFETs operating as freewheeling diode).

With the increase of reverse voltage, a longer time interval is needed to produce a wider space-charge region for supporting the voltage, accompanied by a larger peak reverse recovery current. Evidently, the $I_{\rm rm}$ of Si MBD increases by 2.20 A from 44.56 to 46.76 A. In comparison, the $I_{\rm rm}$ increase of three SiC diodes is nearly zero. As a result, the $I_{\rm rm}$ of SiC SBD (SiC MBD-A and SiC MBD-B) is nearly constant as 3.70 A (4.18 A and 4.99 A). As illustrated in Fig. 18, the $Q_{\rm rr}$ of four DUTs increases linearly with bus voltage. The voltage coefficient of three SiC diodes is 70.4, 87.2, and 52.6 nC/kV, respectively. The voltage coefficient of Si MBD (2131.4 nC/kV) is much larger than that of SiC diodes. Moreover, the absolute value of $Q_{\rm rr}$ of Si MBD is greater than 100 times $Q_{\rm rr}$ of SiC diodes.

The voltage level dependence of $E_{\rm sw}$ is calculated and shown in Fig. 19. Consistent with reverse recovery charge characteristics, the $E_{\rm sw}$ of four DUTs almost increases linearly with reverse

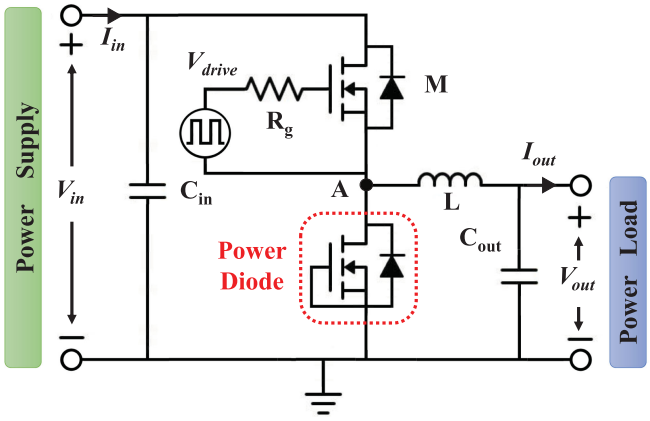

Fig. 20. Schematic of hard switching non-isolated dc–dc buck converter.

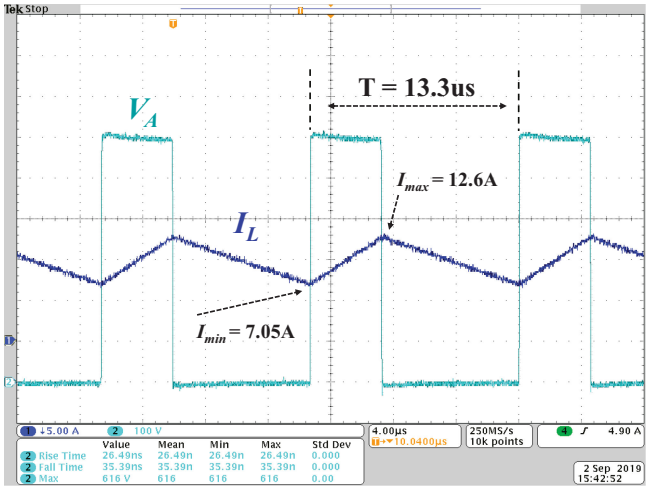

Fig. 21. Measured middle point voltage (V_A) and power inductor current (I_L) while taking the SiC MBD-A as freewheel diode: $V_{\rm in} = 600$ V, $V_{\rm out} = 200$ V, $P_{\rm out} = 2$ kW, $f_{\rm sw} = 75$ kHz and $T = 90$ K. Scale: $V_A = >100$ V/div and $I_L = >5$ A/div. Measured: rise time (and fall time) of V_A is 26.49 ns (and 35.39 ns).

bias voltage. The absolute $E_{\rm sw}$ value of Si MBD is larger than 370 μJ with a variation of 211.11 μJ, while that of SiC diodes is less than 36.11 μJ with a variation of 18.64 μJ.

Although all $E_{\rm sw}$ of four DUTs exists a positive voltage coefficient, the much smaller absolute value and increase the ratio of three SiC diodes fully demonstrate the application potential. Particularly, the SiC MBDs almost have the same performance as the SiC SBD.

V. Continuous Operation Performance of SiC Power Diodes for Cryogenic Application

To quantify the continuous operation performance of SiC MBD and SiC Schottky diode in the actual cryogenic converter, a hard switching nonisolated dc–dc buck converter is designed, with the operation temperature setting capability from 90 K to room temperature (298 K). Importantly, for a fair comparison, the SiC SBD and SiC MBD based buck converters are established using the same double layer PCB, with all other components being identical except the SiC power diodes.

A. Hard Switching Nonisolated DC–DC Buck Converter

Considering the practical application requirements of 1.2-kV power devices, the input voltage of the buck converter is set at 600 V with 34% duty ratio. The converter works in the continuous current mode with the open-loop control method. As shown in Fig. 20, the converter includes the power inductor (L) of 320 μH, the input capacitor ($C_{\rm in}$) of 42.3 μF, the output capacitor ($C_{\rm out}$) of 14.1 μF, the SiC MOSFET (C2M0080120D), and power diode. The power diode in buck converter has been evaluated in the previous section, as SiC SBD and SiC MBD-A. Noted that only the power diode is attached with a large copper plate cooled with liquid nitrogen in the vacuum chamber, while the rest components operate under room temperature.

The typical operation waveforms of 2 kW dc–dc buck are illustrated in Fig. 21, including power inductor current (I_L) and middle point voltage (V_A). Based on the measured I_L, varying linearly between 7.05 and 12.6 A with 5.55-A current ripple, the RMS value of output current can be calculated as 9.95 A. The rise time (and fall time) of V_A is 26.49 ns (and 35.39 ns), indicating that the *dv/dt* for power devices is about 18.12 V/ns and 13.56 V/ns at switching transient.

The total power losses ($P_{\rm loss}$) of buck converter can be split into five parts, including the conduction loss ($P_{\rm Mcon}$) and switching loss ($P_{\rm Msw}$) of power MOSFET, the conduction loss ($P_{\rm Dcon}$) and reverse recovery loss ($P_{\rm Drec}$) of power diode, and passive devices loss ($P_{\rm passive}$), as expressed by the following equation:

$$P_{\rm loss} = P_{\rm Mcon} + P_{\rm Msw} + P_{\rm Dcon} + P_{\rm Drec} + P_{\rm passive}. \quad (9)$$

To evaluate the power conversion performance associated with power loss, the power conversion efficiency (η) is always calculated based on the measured results as

$$\eta = \frac{P_{\rm in}}{P_{\rm out}} \quad (10)$$

where the input power ($P_{\rm in}$) is the product of input voltage ($V_{\rm in}$) and current ($I_{\rm in}$), while the output power ($P_{\rm out}$) is the product of output voltage ($V_{\rm out}$) and current ($I_{\rm out}$).

B. Temperature Dependence Analysis

Since only the power diode is attached to the temperature unit when conducting temperature correlation characterization, the $P_{\rm Dcon}$ and $P_{\rm Drec}$ are only temperature-dependent terms in (9). The characterization results in Section IV clearly show that the $P_{\rm Drec}$ of both SiC SBD and SiC MBD nearly is a nontemperature sensitive parameter at cryogenic temperature. That means the temperature influence on the whole conversion system only comes from conduction loss of power diode. Therefore, (9) can be transformed with more targeted forms reflecting temperature influence as follows:

$$P_{\rm loss} = P_{\rm Dcon}(T) + P_{{\rm non}-T} \quad (11)$$

where the $P_{{\rm non}-T}$ represents the nontemperature sensitive power losses, including $P_{\rm Mcon}$, $P_{\rm Msw}$, $P_{\rm Drec}$, and $P_{\rm passive}$. Since

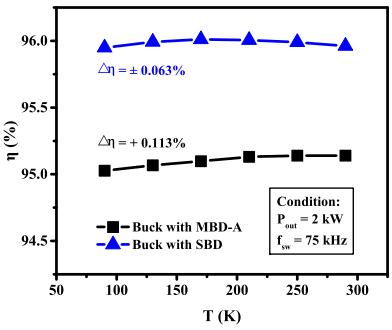

Fig. 22. Comparison of conversion efficiency variation over temperature range from 90 to 298 K with 40 K temperature step. Operation conditions: $P_{\rm out} = 2$ kW, $f_{\rm sw} = 75$ kHz.

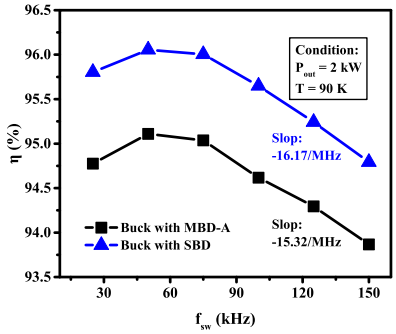

Fig. 23. Comparison of conversion efficiency variation over switching frequency scale. Operation conditions: $P_{\rm out} = 2$ kW, $T = 90$ K.

only the $P_{\rm Dcon}$ is the temperature-sensitive parameter, the temperature dependence on η increase ratio is mainly determined by the forward I-V characteristics of SiC MBD-A and SiC SBD. Fig. 5(a) illustrates that the forward voltage drop of SiC MBD-A increases much more under lower temperature conditions, from 6.64 to 4.16 V at I_f of 10 A. As a result, the increase ratio of η is significantly larger at a lower temperature. In comparison, the almost constant forward voltage drop of SiC SBD, nearly about 1.70 V, as seen in Fig. 7(a) produces a nontemperature dependent of η under the low-temperature scale.

As shown in Fig. 22, the above power loss analysis has been experimentally verified. When the 2-kW buck converters operate with 75-kHz switching frequency over the temperature range from 90 K to room temperature (298 K), the conversion efficiency of MBD-A based converter shows a positive temperature coefficient of $+0.113\%$ increasing from 95.03% to 95.14%. In contrast, the η of SBD-based buck is nearly constant, only existing a value variation of 0.063% with the maximum peak of 96.01% at 170 K. Moreover, the two SiC power diode based buck converters exhibit high enough power conversion efficiency, accompanied by a small efficiency difference (less than 1%).

The small variation results in an almost constant junction temperature cycle amplitude (ΔT_j) for different temperature applications, indicating that the reduction of operating temperature (208 K) can be treated as the reduction of the mean junction temperature $T_{\rm jm}$ over the temperature range from 298 to 90 K. Based on the lifetime model of power device (Coffin–Manson formula), the large acceleration factor (calculated as 3.3^{10}) indicates an extremely promising lifetime of power device [41], [42]. The theoretical lifetime of power device under 90 K can be increased by 10 orders of magnitude when comparing with room temperature case. However, the actual lifetime of the power device is heavily related to the package robustness. The poor package would seriously limit the device lifetime even though the power chip has a promising performance at cryogenic temperature. Therefore, the cryogenic packaging technology is essential to fully realize the application potential of SiC power diodes, thereby extending the device lifetime for cryogenic application.

The sufficiently high energy conversion efficiency (>95%) experimentally validates the potential of SiC power diodes for cryogenic applications and demonstrates the possibility of utilizing the SiC MBD to improve the power density with high conversion efficiency as SiC SBD.

C. Operation Frequency Dependence Analysis

When the buck converter operates with a lower switching frequency, a larger output current ripple increases the RMS value of output current. This causes the conduction power losses (P_{con}), including $P_{\rm Mcon}$ and $P_{\rm Dcon}$, to dominate at low frequency, and eventually produces a decreasing trend of conversion efficiency. In contrast, the proportion of switching losses $(P_{\rm sw})$ is rapidly enhanced at the high switching frequency. The increase of $P_{\rm sw}$ is mainly introduced by $P_{\rm Msw}$ since the $P_{\rm Drec}$ is negligible at cryogenic temperature, as evidenced by previous switching performance characterization. As a result, the conversion efficiency theoretically exists a maximum peak in the intermediate frequency region.

As shown in Fig. 23, the conversion efficiency of a 2-kW buck converter is extracted at 90 K over the frequency scale from 25 to 150 kHz. Both efficiency curves have a peak and similar frequency dependence. Under low-frequency range (<50 kHz), the η of MBD-A based buck (and SBD based buck) increases up to 95.11% (and 96.00%) at 50 kHz from 94.78% (and 95.80%) at 25 kHz. On the contrary, the η of MBD-A based buck (and SBD based buck) linearly decreases from 95.04% (and 96.00%) at 75 kHz to 93.87% (and 94.79%) at 150 kHz. In particular, the absolute drop ratio of η for MBD-A-based buck is 15.32/MHz and smaller than that of SBD based buck (16.17/MHz), indicating that the MBD-A-based buck will get closer and closer to the SBD-based buck with the increase of frequency. Predictably, the η difference of two bucks is only 0.637% while switching frequency increases up to 500 kHz.

The above-mentioned quantitative analysis results demonstrate that the switching frequency has a similar influence on SiC SBD and SiC MBD based cryogenic converters over the wide frequency range, accompanying an optimal switching frequency point.

D. Power Level Dependence Analysis

For buck converter, the five power loss terms are all current dependent functions and increase with power level. It indicates a negative current coefficient for power conversion efficiency.

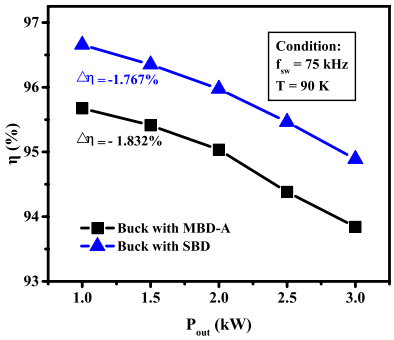

Fig. 24. Comparison of conversion efficiency variation under different output power level. Operation conditions of buck converter: $f_{\rm sw} = 75$ kHz, $T = 90$ K.

Particularly, the $P_{\rm Mcon}$ and $P_{\rm Dcon}$ quadratically increase with output current, calculated by

$$P_{\rm Mcon} = {I_{\rm out}}^2 \times R_{\rm on} \times \frac{V_{\rm out}}{V_{\rm in}} \tag{12}$$

and

$$P_{\rm Dcon} = R_{\rm in0} {I_{\rm out}}^2 + V_{F0} \times I_{\rm out} \tag{13}$$

where $R_{\rm on}$ is the ON-state resistance of MOSFET, $R_{\rm in0}$ is the equivalent series resistance of power diode and can be extracted as reciprocal of forward conductance, V_{F0} is the intrinsic forward voltage drop and can be extracted as forward intercept voltage in forward I-V curve. The above two equations clearly show the $P_{\rm Mcon}$ and $P_{\rm Dcon}$ would dramatically increase at the high current level and become the dominant portion in whole power loss.

To evaluate the high-power performance of the cryogenic buck converter, the power conversion efficiency is extracted under different power levels, as shown in Fig. 24. The two efficiency curves are almost parallel, with the variation of -1.832% and -1.767%. When the output power ($P_{\rm out}$) increases from 1 to 3 kW, the η of MBD-A-based buck (and SBD-based buck) decreases from 95.67% (and 96.66%) to 93.84% (and 94.89%).

The almost consistent downward trend of η reveals that the current level enhancement results in the same energy loss increase for two SiC buck converter. Consequently, the SiC MBD can be used as a free-wheeling diode in the cryogenic power converter, like SiC SBD.

VI. Conclusion

The motivation of this article is to gain insight into the temperature characteristics of SiC power diodes over an ultra-wide temperature scale from 90 to 478 K, with attention to the cryogenic temperature range. The goal of this study is to try to analyze and find out the physical mechanism of electrical performance degradation. Based on a customized temperature characterization platform, the temperature dependence of 1.2-kV SiC MOSFETs' body diode and 1.2 kV SiC SBD are systematically evaluated and analyzed, accompanying with comparative characterizations of 900 V Si CoolMOS's body diode.

The characterization results of the static performance show that temperature reduction degrades the forward characteristics of MBDs while that of SiC SBD shows nonmonotonic change with a minimum value. Particularly, the gate bias voltage can be used to regulate the forward characteristics of SiC MBDs while the SiC SBD and Si MBD do not have this feature. Their regulation ability is more pronounced under low-temperature conditions. Besides, at cryogenic temperature, smaller reverse leakage current can help to improve the reverse blocking performance and smaller junction capacitance is more conducive to the switching operation for high-frequency application.

The characterization results of reverse recovery performance show that temperature reduction facilitates the reverse recovery process of power diodes. Especially, the $I_{\rm rm}$, $Q_{\rm rr}$, and $E_{\rm sw}$ of two SiC MBDs are comparable to the SiC SBD at cryogenic temperature, while SiC diodes offer benefits compared with Si MBD over the temperature range of 90–478 K. Moreover, the reverse recovery performance of SiC MBDs is better than Si MBD. It is comparable to SiC SBD under the switching speed range of 62.3–2054.8 A/μs, with the current range of 6–30 A, and voltage range of 400–1000 V.

Based on two cryogenic hard switching nonisolated dc–dc buck converters, the continuous operation performance of SiC power diodes is evaluated and quantified. The power conversion efficiency of two power converters is greater than 95% over the temperature range from 90 to 298 K. The simplified method and expressions for accurate power loss analysis are proposed and have been experimentally validated at cryogenic temperature, which could reflect the dominant part in total energy loss for the cryogenic converter more concisely. Importantly, the comparative characterization results of two cryogenic buck converters demonstrate the excellent application potential of SiC MBD in cryogenic power conversion system from different dimensions, including operation temperature scale from 90 to 298 K, switching frequency scale from 25 to 150 kHz, and power level scale from 1 to 3 kW.

References

[1] K. Rajashekara and B. Akin, "Cryogenic power conversion systems: The next step in the evolution of power electronics technology," *IEEE Electrific. Mag.*, vol. 1, no. 2, pp. 64–73, Dec. 2013.

[2] K. Rajashekara and B. Akin, "A review of cryogenic power electronics—Status and applications," in *Proc. Int. Electric Mach. Drives Conf.*, 2013, pp. 899–904.

[3] M. Elbuluk, A. Hammoud, and R. Patterson, "Power electronic components, circuits and systems for deep space missions," in *Proc. IEEE 36th Power Electron. Spec. Conf.*, 2005, pp. 1156–1162.

[4] M. Elbuluk and A. Hammoud, "Power electronics in harsh environments," in *Proc. 14th IAS Annu. Meet. Conf. Record Ind. Appl. Conf.*, 2005, vol. 2, pp. 1442–1448.

[5] M. Frank *et al.*, "High-temperature superconducting rotating machines for ship applications," *IEEE Trans. Appl. Supercond.*, vol. 16, no. 2, pp. 1465–1468, Jun. 2006.

[6] N. Maki, M. Izumi, M. Numano, K. Aizawa, K. Okumura, and K. Iwata, "Design study of high-temperature superconducting motors for ship propulsion systems," in *Proc. Int. Conf. Electr. Mach. Syst.*, 2007, pp. 1523–1527.

[7] B. J. Baliga, *Silicon Carbide Power Devices*. Singapore: World Scientific, 2006.

[8] J. Millán, P. Godignon, X. Perpiñà, A. Pérez-Tomás, and J. Rebollo, "A survey of wide bandgap power semiconductor devices," *IEEE Trans. Power Electron.*, vol. 29, no. 5, pp. 2155–2163, May 2014.

[9] X. Yuan, "Application of silicon carbide (SiC) power devices: Opportunities, challenges and potential solutions," in *Proc. 43rd Annu. Conf. IEEE Ind. Electron. Soc.*, 2017, pp. 893–900.

[10] X. She, A. Q. Huang, Ó. Lucía, and B. Ozpineci, "Review of silicon carbide power devices and their applications," *IEEE Trans. Ind. Electron.*, vol. 64, no. 10, pp. 8193–8205, Oct. 2017.
[11] J. Qi *et al.*, "Temperature dependence of dynamic performance characterization of 1.2-kV SiC Power MOSFETs compared with Si IGBTs for wide temperature applications," *IEEE Trans. Power Electron.*, vol. 34, no. 9, pp. 9105–9117, Sep. 2019.
[12] T. Funaki *et al.*, "Characterization of SiC diodes in extremely high temperature ambient," in *Proc. 21st Annu. IEEE Appl. Power Electron. Conf. Expo.*, 2006, pp. 9105–9117.
[13] T. Funaki *et al.*, "Power conversion with SiC devices at extremely high ambient temperatures," *IEEE Trans. Power Electron.*, vol. 22, no. 4, pp. 1321–1329, Jul. 2007.
[14] K. Peng, S. Eskandari, and E. Santi, "Characterization and modeling of SiC MOSFET body diode," in *Proc. IEEE Appl. Power Electron. Conf. Expo.*, 2016, pp. 2127–2135.
[15] V. Pala *et al.*, "Physics of bipolar, unipolar and intermediate conduction modes in silicon carbide MOSFET body diodes," in *Proc. 28th Int. Symp. Power Semicond. Devices ICs*, 2016, pp. 227–230.
[16] R. Radhakrishnan, T. Witt, and R. Woodin, "Temperature dependent design of silicon carbide Schottky diodes," in *Proc. IEEE Workshop Wide Bandgap Power Devices Appl.*, 2014, pp. 151–154.
[17] O. Alatise, N. Parker-Allotey, and P. Mawby, "The dynamic performance of SiC Schottky Barrier diodes with parasitic inductances over a wide temperature range," in *Proc. 6th IET Int. Conf. Power Electron. Mach. Drives*, 2012, pp. 1–6.
[18] O. Alatise, N. Parker-Allotey, D. Hamilton, and P. Mawby, "The impact of parasitic inductance on the performance of silicon–carbide schottky barrier diodes," *IEEE Trans. Power Electron.*, vol. 27, no. 8, pp. 3826–3833, Aug. 2012.
[19] S. Jahdi *et al.*, "An analysis of the switching performance and robustness of power MOSFETs body diodes: A technology evaluation," *IEEE Trans. Power Electron.*, vol. 30, no. 5, pp. 2383–2394, May 2015.
[20] X. Zhang, L. Gant, G. Sheh, and S. Banerjee, "Characterization and optimization of SiC freewheeling diode for switching losses minimization over wide temperature range," in *Proc. PCIM Eur. Int. Exh. Conf. Power Electron. Intell. Motion, Renewable Energy Energy Manage.*, 2017, pp. 1–7.
[21] M. R. Ahmed, R. Todd, and A. J. Forsyth, "Switching performance of a SiC MOSFET body diode and SiC schottky diodes at different temperatures," in *Proc. IEEE Energy Convers. Congress Expo.*, 2017, pp. 5487–5494.
[22] X. Hou, D. Boroyevich, and R. Burgos, "Characterization on latest-generation SiC MOSFET's body diode," in *Proc. IEEE 4th Workshop Wide Bandgap Power Devices Appl.*, 2016, pp. 247–252.
[23] A. E. Awwad and S. Dieckerhoff, "Operation of planar and trench SiC MOSFETs in a 10 kW DC/DC-converter analyzing the impact of the body diode," in *Proc. IEEE Energy Convers. Congress Expo.*, 2017, pp. 917–924.
[24] G. Spiazzi, S. Buso, M. Citron, M. Corradin, and R. Pierobon, "Performance evaluation of a Schottky SiC power diode in a boost PFC application," *IEEE Trans. Power Electron.*, vol. 18, no. 6, pp. 1249–1253, Nov. 2003.
[25] Z. Zhang, B. Guo, F. F. Wang, E. A. Jones, L. M. Tolbert, and B. J. Blalock, "Methodology for wide band-gap device dynamic characterization," *IEEE Trans. Power Electron.*, vol. 32, no. 12, pp. 9307–9318, Dec. 2017.
[26] A. Anthon, J. C. Hernandez, Z. Zhang, and M. A. E. Andersen, "Switching investigations on a SiC MOSFET in a TO-247 package," in *Proc. 40th Annu. Conf. IEEE Ind. Electron. Soc.*, 2014, pp. 1854–1860.
[27] D. Reusch and J. Strydom, "Understanding the effect of PCB layout on circuit performance in a high-frequency gallium-nitride-based point of load converter," *IEEE Trans. Power Electron.*, vol. 29, no. 4, pp. 2008–2015, Apr. 2014.
[28] Y. Ren *et al.*, "Voltage suppression in wire-bond-based multichip phase-leg SiC MOSFET module using adjacent decoupling concept," *IEEE Trans. Ind. Electron.*, vol. 64, no. 10, pp. 8235–8246, Oct. 2017.
[29] J. C. Hernandez, L. P. Petersen, M. A. E. Andersen, and N. H. Petersen, "Ultrafast switching superjunction MOSFETs for single phase PFC applications," in *Proc. IEEE Appl. Power Electron. Conf. Expo.*, 2014, pp. 143–149.
[30] S. Yin, Y. Liu, Y. Liu, K. J. Tseng, J. Pou, and R. Simanjorang, "Comparison of SiC voltage source inverters using synchronous rectification and freewheeling diode," *IEEE Trans. Ind. Electron.*, vol. 65, no. 2, pp. 1051–1061, Feb. 2018.
[31] M. Shen and S. Krishnamurthy, "Simplified loss analysis for high speed SiC MOSFET inverter," in *Proc. 27th Annu. IEEE Appl. Power Electron. Conf. Expo.*, 2012, pp. 1682–1687.
[32] R. Raghunathan and B. J. Baliga. "Temperature dependence of hole impact ionization coefficients in 4H and 6H-SiC," *Solid-State Electron.*, vol. 43, no. 2, pp. 199–211, 1999.
[33] D. Sadik, J. Lim, P. Ranstad, and H. Nee, "Investigation of long-term parameter variations of SiC power MOSFETs," in *Proc. 17th Eur. Conf. Power Electron. Appl.*, 2015, pp. 1–10.
[34] L. Fursin, X. Li, Z. Li, M. O'Grady, W. Simon, and A. Bhalla, "Reliability aspects of 1200V and 3300V silicon carbide MOSFETs," in *Proc. IEEE 5th Workshop Wide Bandgap Power Devices Appl.*, 2017, pp. 373–377.
[35] Y. Ebiike *et al.*, "Reliability investigation with accelerated body diode current stress for 3.3 kV 4H-SiC MOSFETs with various buffer epilayer thickness," in *Proc. IEEE 30th Int. Symp. Power Semicond. Devices ICs*, 2018, pp. 447–450.
[36] R. Fujita, K. Tani, K. Konishi, and A. Shima, "Failure of switching operation of SiC-MOSFETs and effects of stacking faults on safe operation area," *IEEE Trans. Electron Devices*, vol. 65, no. 10, pp. 4448–4454, Oct. 2018.
[37] R. E. Stahlbush, K. N. A. Mahakik, A. J. Lelis, and R. Green, "Effects of basal plane dislocations on SiC power device reliability," in *Proc. IEEE Int. Electron Devices Meet.*, 2018, pp. 19.4.1–19.4.4.
[38] B. J. Baliga, *Fundamentals of Power Semiconductor Devices*. New York, NY, USA: Springer-Verlag, 2008.
[39] T. Kimoto and J.A. Cooper, "Appendix A: Incomplete dopant ionization in 4H-SiC," in *Fundamentals of Silicon Carbide Technology: Growth, Characterization, Devices and Applications*. Piscataway, NJ, USA: IEEE, 2014, pp. 511–515.
[40] J. Vuillod, "Modeling and analysis of temperature dependence of the concentration and mobility of charge carriers in SiC layers. Determination of the compensation ratio," in *Proc. Int. Conf. Microelectron.*, 1995, vol. 1, pp. 101–106.
[41] D.Zhou F. Blaabjerg, T. Franke, M. Tønnes, and M. Lau, "Comparison of wind power converter reliability with low-speed and medium-speed permanent-magnet synchronous generators," *IEEE Trans. Ind. Electron.*, vol. 62, no. 10, pp. 6575–6584, Oct. 2015.
[42] L. Ceccarelli, R. M. Kotecha, A. S. Bahman, F. Iannuzzo, and H. A. Mantooth, "Mission-profile-based lifetime prediction for a SiC mosfet power module using a multi-step condition-mapping simulation strategy," *IEEE Trans. Power Electron.*, vol. 34, no. 10, pp. 9698–9708, Oct. 2019.

Jinwei Qi (Student Member, IEEE) received the B.S. degree in microelectronics and solid-state electronics in 2015 from Xi'an Jiaotong University, Xi'an, China, where he is currently working toward the Ph.D. degree in electronic science and technology.

He has been visiting the Department of Engineering – Electrical Engineering Division, University of Cambridge, Cambridge, U.K., as a Visiting Ph.D. Scholar from September 2019. His current research interests include wide bandgap device modeling and reliability analysis under ultra-wide temperature scales.

Xu Yang (Senior Member, IEEE) received the B.S. and Ph.D. degrees in electrical engineering from Xi'an Jiaotong University, Xi'an, China, in 1994 and 1999, respectively.

Since 1999, he has been a member of the Faculty with the School of Electrical Engineering, Xi'an Jiaotong University, where he is currently a Professor. From 2004 to 2005, he was with the Center of Power Electronics Systems, Virginia Polytechnic Institute and State University, Blacksburg, VA, as a Visiting Scholar. He then came back to Xi'an Jiaotong University. His research interests include soft switching topologies, PWM control techniques and power electronic integration, and packaging technologies.

Xin Li received the M. S. and Ph.D. degrees from Xi'an Jiaotong University, Xi'an, China, in 2000 and 2004, respectively.

She has been a Professor with the School of Electronic and Information Engineering, Xi'an Jiaotong University. So far, she has published more than 30 peer-reviewed journal papers. Her research interests include molecular electronic device, carbon-based electronics, graphene/carbon nanotube composite sensor, biochips & microfluidics, smart structures and micro/nanostructures, and vacuum nano electronic devices.

Dr. Li is Reviewer for "*Nanoscale*," and "*Sensors and Actuators B*," etc.

Wenjie Chen (Senior Member, IEEE) received the B.S., M.S., and Ph.D. degrees in electrical engineering from Xi'an Jiaotong University, Xi'an, China, in 1996, 2002, and 2006, respectively.

Since 2002, she has been a member of the Faculty with the School of Electrical Engineering, Xi'an Jiaotong University, where she is currently a Professor. From 2012 to 2013, she was with the Department of Electrical Engineering and Computer Science, University of Tennessee, Knoxville, TN, USA, as a Visiting Scholar. She then came back to Xi'an Jiaotong University and engaged in the teaching and research in power electronics. Her main research interests include electromagnetic interference, active filters, and power electronic integration.

Kai Tian (Student Member, IEEE) received the B.S. degree in engineering from Northwestern Polytechnical University, Xi'an, China, in 2013, the M.S. degree in engineering from Harbin Engineering University, Harbin, China, in 2015, and the Ph.D. degree in electrical engineering from Xi'an Jiaotong University, Xi'an, China, in 2019.

He visited the Royal Institute of Technology in Sweden, as a Guest Ph.D. Scholar from March 2018 to February 2019. His research interests include SiC-based power devices, design, modeling and characterization of the SiC-based power MOSFET, and PiN diode.

Menghua Wang received the B.S. degree in microelectronics and solid-state electronics from Xi'an University of Posts & Telecommunications, Xi'an, China, in 2017. She is currently working toward the Ph.D. degree in electronic science and technology with the Xi'an Jiaotong University, Xi'an, China.

Her research interests include SiC-based power devices and reliability analysis and characterization of the SiC-based power MOSFET.

Shuwen Guo received the B.S. degree from the College of Physics and Electronic Engineering, Chongqing Normal University, Chongqing, China, in 2017. She is currently working toward the Ph.D. degree in electronic science and technology with Xi'an Jiaotong University, Xi'an, China.

Her research interests include SiC-based power devices, including the UV detection based on 4H SiC APD.

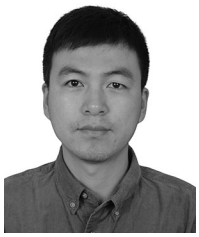

Mingchao Yang received the B.S. and M.S. degrees in engineering from Xi'an University of Technology, Xi'an, China, in 2009 and 2012, respectively.

From 2012 to 2015, he worked with Jingjing Optoelectronic Technology Co., Ltd. Since 2016, he has been a member with the School of Microelectronic, Xi'an Jiaotong University. His main area of research focuses on wide band gap devices.